4632–4641 *Nucleic Acids Research, 2017, Vol. 45, No. 8* *Published online 31 March 2017*
doi: 10.1093/nar/gkx206

A DEAD-box protein acts through RNA to promote HIV-1 Rev-RRE assembly

Rajan Lamichhane[1], John A. Hammond[1], Raymond F. Pauszek, III[1], Rae M. Anderson[2], Ingemar Pedron[1], Edwin van der Schans[1], James R. Williamson[1] and David P. Millar[1,*]

[1]Department of Integrative Structural and Computational Biology, The Scripps Research Institute, La Jolla, CA 92037, USA and [2]Department of Physics, University of San Diego, San Diego, CA 92110, USA

Received January 18, 2017; Revised March 14, 2017; Editorial Decision March 19, 2017; Accepted March 28, 2017

ABSTRACT

The HIV-1 Rev protein activates nuclear export of unspliced and partially spliced viral RNA transcripts, which encode the viral genome and the genes encoding viral structural proteins, by binding to and oligomerizing on the Rev Response Element (RRE). The human DEAD-box protein 1 (DDX1) enhances the RNA export activity of Rev through an unknown mechanism. Using a single-molecule assembly assay and various DDX1 mutants, we show that DDX1 acts through the RRE RNA to specifically accelerate the nucleation step of the Rev-RRE assembly process. Single-molecule Förster resonance energy transfer (smFRET) experiments using donor-labeled Rev and acceptor-labeled DDX1 show that both proteins can associate with a single RRE molecule. However, simultaneous interaction is only observed in a subset of binding events and does not explain the extent to which DDX1 promotes the nucleation step of Rev-RRE assembly. Together, these results are consistent with a model wherein DDX1 acts as an RNA chaperone, remodeling the RRE into a conformation that is pre-organized to bind the first Rev monomer, thereby promoting the overall Rev-RRE assembly process.

INTRODUCTION

During the late stage of HIV-1 infection, unspliced viral RNA transcripts must be exported from the nucleus to the cytoplasm, either to be translated into structural proteins or to provide the genomic RNA needed for packaging into new virions. Since incompletely spliced RNAs are usually retained in the nucleus, a specialized viral protein, known as Rev (Regulator of Expression of Virion (1)), is used to promote export of unspliced and singly spliced viral transcripts to the cytoplasm via the CRM1 (chromosome maintenance region 1) pathway (2). Rev interacts with a highly conserved intronic RNA element, the Rev Response Element (RRE), which consists of an extended duplex region (stem I) and four or five stem-loop elements (Figure 1A). The Rev protein contains an RNA-binding domain and nuclear localization signal, flanked by regions required for oligomerization, and a nuclear export signal recognized by CRM1 (Figure 1B). The presence of multiple Rev monomers bound to the RRE is required for efficient export activity (3,4).

The assembly of the Rev-RRE complex has been extensively characterized using both biochemical and biophysical methods. Assembly is initiated by the binding of a single Rev monomer to a high affinity site in stem IIB (Figure 1A) (5–7) and proceeds by incorporation of additional Rev monomers into the ribonucleoprotein complex (8–10), which are recruited one at a time through a combination of protein–RNA and protein–protein interactions (11). Kinetic parameters describing each step of Rev-RRE assembly or disassembly have been determined through single-molecule studies (11,12). A secondary Rev binding site was identified in stem IA of the RRE (10) and a model for the three-dimensional architecture of the RRE has been proposed on the basis of small-angle X-ray scattering studies (13).

In addition to proteins involved in the CRM1 export pathway, a variety of other host proteins are also known to affect Rev function (reviewed in ref (14)). In particular, the DEAD-box protein DDX1 has been implicated as a key cellular cofactor of Rev (15–17). DDX1 is required for efficient Rev function and proper nuclear localization of Rev in mammalian cells (15) and human astrocytes (18,19). Proteomic analysis by mass spectrometry has identified DDX1 as an interaction partner of Rev (16). Importantly, silencing of DDX1 in HIV-1 infected human cells markedly reduces virus particle production (17).

Similar to other DEAD-box proteins, DDX1 contains a Q motif and a helicase core consisting of N-terminal and C-terminal RecA-like domains (Figure 1C). As expected, DDX1 exhibits RNA-dependent ATPase activity characteristic of other members of the DEAD-box family (17). However, DDX1 is unique in also containing a SPRY do-

*To whom correspondence should be addressed. Tel: +1 858 784 9870; Fax: +1 858 784 9067; Email: millar@scripps.edu

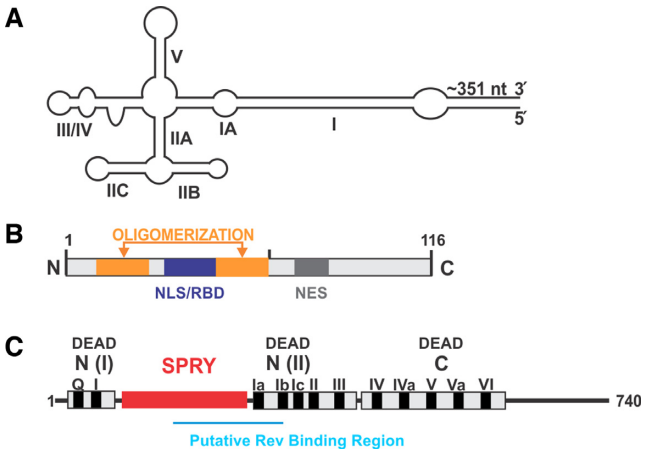

Figure 1. Experimental system. (**A**) Schematic diagram of the full-length RRE, showing the various secondary structure elements. (**B**) Domain organization of HIV-1 Rev, showing the regions required for oligomerization (orange), RNA binding (RBD, blue) and the locations of the nuclear localization signal (NLS, blue) and nuclear export signal (NES, grey). (**C**) Schematic illustration of DDX1. Structural domains DEAD N-term, SPRY and DEAD C-term are shown in boxes and labeled above. Conserved DEAD-box motifs are shown in black and labeled Q-VI. The putative Rev binding region is underlined in blue.

main between the Q motif and the N-terminal helicase domain (Figure 1C). Yeast-two-hybrid experiments suggest that an N-terminal region of Rev interacts with DDX1 (15) and direct *in vitro* binding studies have demonstrated high affinity association between DDX1 and Rev (17).

While the DDX1-Rev protein–protein interaction has been well documented, much less is known about whether DDX1 can act upon RNA during the HIV-1 life cycle. DEAD-box proteins are involved in many aspects of RNA metabolism, including ribosome biogenesis, RNA splicing, translation and RNA degradation (20,21), though their mechanistic role in these processes remain largely elusive. In a previous single-molecule study, we provided evidence that DDX1 promotes Rev-RRE assembly *in vitro* (12). However, understanding the role of DDX1 during Rev-RRE assembly is complicated by the fact that DDX1 can physically interact with the Rev protein or the RRE RNA (17). The purpose of this study is to identify the relevant DDX1 interaction partner and to dissect the mechanism by which DDX1 promotes Rev-RRE assembly. We demonstrate that DDX1 acts through the RRE rather than Rev to accelerate the nucleation step of Rev-RRE assembly. Moreover, our results suggest that DDX1 does not need to be physically present on the RRE to promote assembly. The results presented in this work are consistent with a model in which DDX1 acts as an RNA folding chaperone, producing an altered RRE species that is optimized for the first Rev monomer binding event.

MATERIALS AND METHODS

Rev expression, purification and labeling

A Rev protein construct with the two native cysteines removed (via C85S and C89S mutations) and with a N-terminal extension containing a hexahistidine tag and a single cysteine residue was expressed, purified and labeled with Alexa Fluor 555 (A555) maleimide, as described (12). Labeled and unlabeled Rev proteins were separated by HPLC purification under denaturing conditions, and the labeled protein was subsequently refolded by equilibrium dialysis in a native buffer (50 mM Tris pH 7.5, 500 mM NaCl, 1 mM EDTA), then divided into small aliquots and stored at −80°C. The degree of A555 labeling, estimated from absorbance measurements at 280 and 555 nm, was >94%.

Preparation of WT DDX1 and DDX1 mutants with ybbR tag

Since DDX1 contains multiple cysteine residues it is not possible to site-specifically label this protein using conventional maleimide chemistry. Instead, we used a previously described enzymatic labeling protocol (22) to attach Alexa Fluor 647 (A647) to a 11 amino acid peptide tag (termed ybbR) fused to the N-terminus of DDX1. The DNA sequence encoding the ybbR tag (GATTCTCTTGAATTTA TTGCTAGTAAGCTTGCG) was inserted into a plasmid containing the DDX1 gene (also including hexahistidine affinity tag) using the QuikChange II protocol (Stratagene) and the forward and reverse primers shown in Supplementary Table S1. Reactions were set up according to the manufacturer's protocol and the insertion of the ybbR tag was confirmed by DNA sequence analysis. The resulting plasmid is called ybbR-DDX1 and the protein expressed from this plasmid is referred to in this paper as wild-type (WT) DDX1. The ybbR-DDX1 plasmid was also used as the template for the preparation of L303E/L322E (Rev binding mutant) and S295E/R296E/T515E-K516E (RNA binding mutant) DDX1 constructs, again using the QuikChange II protocol. For each desired mutant, the individual mutations were introduced sequentially (e.g. to make the Rev binding-deficient DDX1 mutant, L322E was first introduced, then L303E was introduced into the L322E-containing plasmid). All plasmids were sequenced after each mutagenesis step to ensure the desired change was made and that the rest of the gene was error-free.

Expression and purification of WT DDX1 and DDX1 mutants

DDX1-ybbR plasmids (WT and mutants) were transformed into BL21(DE3) CodonPlus RIL cells from Stratagene and cells were grown in LB broth at 37°C. The cultures were transferred into 1 l 2xYT medium and grown at 37°C to an OD_{600} ∼0.8. Afterwards, the cultures were equilibrated at a temperature of 20°C for 10 min and protein expression was induced by addition of 1 mM IPTG. After overnight incubation, cells were harvested by centrifugation and stored at −80°C until ready for use. Expression levels were checked via SDS-PAGE on a 4–20% TGX gel from BioRad. The frozen biomass was resuspended in 30 ml lysis buffer (25 mM Tris pH 8.0, 1 M NaCl, 10% glycerol, 0.1% Triton-X-100, 10 mM imidazole, 3 mM β-mercaptoethanol) with one tablet of cOmplete EDTA-free protease inhibitor from Roche. Chicken egg lysozyme (2 mg/ml) was added to the suspension and left on ice to incubate for at least 1 h. After sonication, cell debris was removed by centrifugation, and the resulting lysate was

treated with 5% polyethyleneimine (Sigma) to remove contaminating nucleic acids prior to affinity column purification using Ni-NTA resin (QIAGEN). The eluted fractions were concentrated to a 1 ml volume on an Amicon 15 cartridge with a MWCO of 50 000 Da. The retentate was diluted in 49 ml of low salt Q column buffer (25 mM Tris pH 8.8, 25 mM NaCl, 2 mM DTT, 1 mM EDTA) and applied to a HiTrap Q HP column. Purified DDX1 was exchanged into storage buffer (25 mM Tris pH 7.5, 500 mM NaCl, 2 mM DTT, 1 mM EDTA) using three spin cycles through an Amicon 4 cartridge (MWCO 30,000 Da) and stored with 50% glycerol in small aliquots at −80°C.

Enzymatic labeling of DDX1 with CoA-647

CoA-647 from New England Biosciences was used to label the ybbR-DDX1, as described previously (22). ybbR-DDX1 in storage buffer was exchanged into labeling buffer (50 mM HEPES pH 7.4, 500 mM NaCl, 10 mM $MgCl_2$, 1 mM DTT). Five nmol of ybbR-DDX1 was mixed with 15 nmol CoA-647 (dissolved in DMSO) and 1 μM Sfp synthase (New England Bioscience) in labeling buffer. The reaction was incubated overnight in the dark at 4°C, then applied to Ni-NTA agarose resin (Qiagen). Labeled DDX1 was eluted from the column with elution buffer (25 mM Tris pH 8.0, 1 M NaCl, 200 mM imidazole, 3 mM β-mercaptoetahanol). The eluted fractions were exchanged into storage buffer (50 mM Tris pH 7.5, 500 mM NaCl, 2 mM DTT, 1 mM EDTA) using an Amicon4 cartridge (MWCO 30 000 Da) and stored with 50% glycerol in small aliquots at −80°C. The degree of A647 labeling, estimated from absorbance measurements at 280 and 650 nm, was 47%.

RRE constructs

A full length BH10 RRE-containing construct is previously described (17). DNA templates for transcription were generated via PCR amplification of the full length (RRE + hybridization sequences, primers listed in Supplementary Table S1). These were then used directly in T7 RNA polymerase transcription reactions as described (23). The desired RNAs were purified from transcription byproducts using denaturing polyacrylamide gel electrophoresis followed by gel crushing and passive elution into RNAse-free water. Resulting RNA purity was verified via denaturing polyacrylamide gel electrophoresis.

DDX1-Rev binding assay

Binding of WT DDX1 or DDX1 mutants to Rev was monitored by fluorescence anisotropy. Mixtures of A555-labeled Rev (30 nM) and increasing concentrations of unlabeled DDX1 were prepared in Rev binding buffer (10 mM HEPES pH7.5, 150 mM KCl, 2 mM $MgCl_2$, 5 mM β-mercaptoethanol and 10% glycerol). The fluorescence anisotropy of A555 in each mixture was recorded in an Envision 2104 multilevel plate reader, with excitation at 535 nm and the emission recorded at 595 nm. The resulting data were fitted to a 1:1 binding model, using the following equation:

$$r = r_F + (r_B - r_F)\left\{\frac{(R_t + D_t + K_d) - \left[(R_t + D_t + K_d)^2 - 4R_t D_t\right]^{1/2}}{2R_t}\right\} \quad (1)$$

where r is the measured anisotropy, R_t is the total concentration of Rev and D_t is the total concentration of DDX1. The anisotropy of free and bound Rev, r_F and r_B, respectively, and the equilibrium dissociation constant for the Rev-DDX1 complex, K_d, were optimized for best fit of Equation (1) to the observed titration data using Igor Pro software (WaveMetrics).

Surface treatment and RNA immobilization

Quartz slides were cleaned, passivated with polyethylene glycol (95% maleimide and 5% biotin) and coated with 20 μg/ml neutravidin, as described (24). The RRE construct (500 pM) was hybridized with biotin-labeled (1 nM) and A647-labeled (2 nM) DNA oligonucleotides, complementary to the 3′ and 5′ extensions, respectively, in annealing buffer (50 mM HEPES, pH 7.5 and 150 mM KCl) by heating to 90°C and slow cooling to room temperature. The resulting mixture in imaging buffer (50 mM HEPES, pH 7.5, 150 mM NaCl, 10 mM K_2SO_4, 2 mM $MgCl_2$, 2 mM DTT, 2 mM trolox, 50 μg/ml glucose oxidase, 10 μg/ml catalase and 2–5% wt/vol glycerol) was applied to the slide surface and an image of the surface was recorded by TIRF microscopy, exciting the A647 probe with a red laser (643 nm). The image revealed hundreds of well-separated discrete red fluorescent spots (not shown), confirming immobilization of the RNA/DNA hybrid. After validating the immobilization scheme, the A647-oligonucleotide was no longer used.

Single-molecule fluorescence data collection

Single-molecule fluorescence data was collected using a custom built prism-based TIRF microscope (Axiovert 200, Zeiss) under oxygen scavenging conditions, as described (25). For single-color experiments, 500 pM RRE–biotin DNA hybrid was premixed with 1 nM A555 labeled Rev, immobilized on the surface and excited with a green laser at 532 nm. In some experiments, 50 nM DDX1 (WT or mutants) was also present. For FRET experiments 500 pM RRE–biotin DNA hybrid was premixed with 1 nM A555-labeled Rev and 50 nM A647-labeled DDX1, immobilized on the surface and excited with a 532 nm laser. All experiments were performed in TIRF imaging buffer. The emission intensities from discrete fluorescent spots on the surface, representing immobilized RNA-protein complexes, were acquired over time on an intensified CCD camera (Andor IXON) with 100 ms resolution. A dual-view optical splitter was used to separate green and red emission channels for the FRET measurements. Custom single-molecule data acquisition software was used to record camera data, identify discrete fluorescent spots in the green channel and the corresponding spot in the red channel (for FRET experiments), and to generate fluorescence intensity versus time traces for each spot or pair of spots.

Single-molecule fluorescence data analysis

All intensity versus time traces were corrected for background and smoothed using 3-point linear averaging. For single-color experiments, multiple A555 emission traces were compiled and used to construct composite intensity histograms, using Igor Pro software (WaveMetrics). Individual time traces were also fitted using Hidden Markov modeling (26) to determine dwell times spent in a given state prior to transition to another state. Histograms of these dwell times were compiled and fitted with a single-exponential function to determine the rate constant for transitions from one state to another, using Igor Pro software (WaveMetrics). In cases where a single-exponential fit was not adequate, based on the reduced chi-square value, the histogram was fitted with a bi-exponential function. The uncertainties in the fitted rate constants were also reported by the software. For FRET analysis, the apparent FRET efficiency at each time point, E_{app}, was calculated according to Equation (2):

$$E_{app} = {I_A}/{(I_D + I_A)} \quad (2)$$

where I_D and I_A are the donor and acceptor emission intensities at the corresponding time point, respectively. Composite histograms of apparent FRET efficiency were compiled from multiple time traces.

RESULTS

Rev-RRE assembly in the presence of WT DDX1 and DDX1 mutants

We used a single-color single-molecule fluorescence assay (11) to monitor Rev-RRE assembly, in the absence or presence of WT DDX1 or specific DDX1 mutants. An RRE construct containing the full 351 nt sequence and short extensions at the 3′ and 5′ ends was prepared by *in vitro* transcription (Supplementary Figure S1A). A biotin-labeled DNA oligonucleotide annealed to the 3′ extension (Supplementary Figure S1A) was used to immobilize the RRE construct on a quartz surface coated with polyethylene glycol (PEG) and neutravidin (Figure 2A). The Rev construct had the two native cysteines removed (via C85S and C89S mutations) and contained a single cysteine residue within an N-terminal extension (full sequence shown in Supplementary Figure S1B), as described (12). This Rev construct was labeled with an A555 fluorophore via the single cysteine residue. The Rev-RRE binding and dissociation rate constants for this labeled Rev construct (12) are similar to those previously reported for Rev labeled at one of the native cysteines and lacking the N terminal extension (11).

Binding of labeled Rev monomers to the surface-immobilized RRE was monitored by TIRF microscopy (Figure 2A). Rev binds specifically to the immobilized RRE, with negligible non-specific surface adsorption (Supplementary Figure S2). A representative fluorescence intensity versus time trace for one immobilized RRE molecule (Figure 2B, left panel) shows discrete intensity jumps as individual Rev monomers (~200 a.u. per monomer) bind to or dissociate from the RRE, one molecule at a time (11). A histogram of fluorescence intensities compiled from 223 such time traces shows separate peaks representing 1:1 and 2:1 Rev-RRE complexes (Figure 2B, right panel). Dwell time analysis reveals that the first Rev monomer binds to the RRE with a first-order rate constant of 0.09 ± 0.01 s^{-1} (Figure 3A), corresponding to a bimolecular association rate constant of (9.0 ± 1.0) × 10^7 M^{-1} s^{-1} at the Rev concentration used (1 nM). In a previous single-molecule study, two distinct kinetic phases were observed during the nucleation step, and these were attributed to heterogeneity in the Rev and/or RRE populations (12). Here, we observe single-exponential kinetics during the nucleation step, implying that the Rev and/or RRE preparations used in the present study are more homogeneous.

Corresponding single-molecule fluorescence data recorded in the presence of 50 nM WT DDX1 is shown in Figure 2C. The representative time trace (left panel) shows stepwise binding of four Rev monomers to the RRE. Relative to Rev alone, the intensity histogram compiled from 132 immobilized RRE molecules (Figure 2C, right panel) shows a marked increase in the 2:1 stoichiometry peak and a pronounced tail extending to higher emission intensities, representing unresolved 3:1 and 4:1 Rev-RRE complexes. Dwell time analysis reveals that the first Rev monomer binds rapidly to the RRE in the presence of DDX1, with a first-order rate constant of 0.84 ± 0.10 s^{-1}, which is ~9-fold faster than observed in the presence of Rev alone (Figure 3B). This acceleration of the first Rev monomer binding step in the presence of DDX1 is more pronounced than reported previously (12). In addition, a minor kinetic phase (first-order rate constant of 0.11 ± 0.04 s^{-1} with amplitude of 6 ± 3%) is also observed during the first Rev monomer binding step. The rate constant is similar to that observed for Rev alone (Figure 3A), suggesting that this phase arises from a small population of Rev and/or RRE molecules that are unaffected by the presence of DDX1.

The preceding results were obtained in the absence of any added ATP. Since DDX1 is an ATP-dependent RNA helicase, a question arises as to whether the acceleration of Rev-RRE binding is even more pronounced in the presence of ATP. Accordingly, smTIRF measurements were performed in the presence of DDX1 and 1 mM ATP. The rate constants describing binding of the first Rev monomer to the RRE are very similar to those observed in the absence of ATP (Supplementary Figures S3 and 3B). Together, these results demonstrate that the ability of DDX1 to accelerate binding of the first Rev monomer to the RRE does not depend on the presence of added ATP.

The ability of DDX1 to accelerate the nucleation step of Rev-RRE assembly could be due to a physical interaction between DDX1 and the Rev protein. Previous biochemical studies have shown direct binding of DDX1 to Rev, in a concentration range similar to conditions of the present experiments (17). To determine whether the ability of DDX1 to promote Rev assembly on the RRE requires a physical interaction between DDX1 and Rev, we made a series of single mutations in the putative Rev-binding region of DDX1 (15) and tested the resulting mutant proteins for Rev binding. Two of the mutations (L303E and L322E, Supplementary Figure S4A) showed defects in Rev binding. We created a DDX1 construct containing both mutations

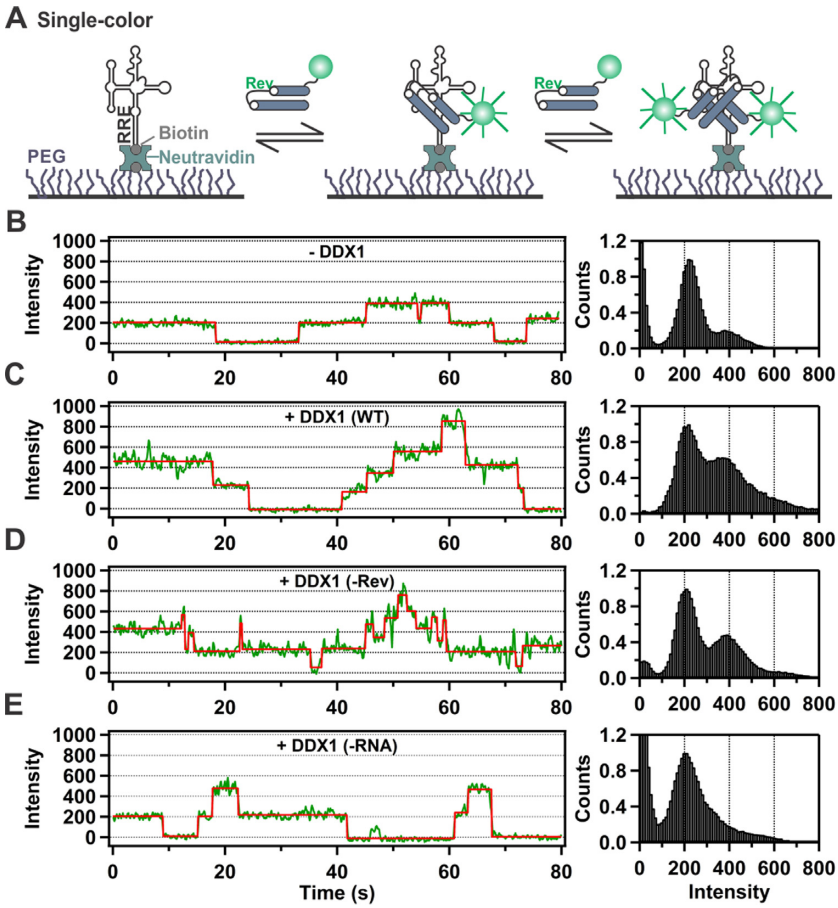

Figure 2. Rev-RRE assembly monitored by single-color TIRF microscopy. (**A**) Schematic of the assembly assay, showing the RRE construct immobilized on a PEG-coated surface by means of biotin–neutravidin attachment. One or more Rev molecules labeled with an A555 fluorophore (green circle) can bind from solution to the immobilized RRE and become fluorescent upon excitation by a totally internally reflected green laser (not shown). (**B**) The left panel shows a representative fluorescence intensity versus time trace (green) recorded in the absence of DDX1 and a corresponding fit to a hidden Markov model (26) (red). The right panel shows a binned histogram of fluorescence intensities compiled from 223 individual intensity-time traces. (**C**) Corresponding data recorded in the presence of 50 nM WT DDX1. The histogram is compiled from 132 individual traces. Other details as in part A. (**D**) Corresponding data recorded in the presence of 50 nM DDX1 (-Rev) mutant. The histogram is compiled from 292 individual traces. Other details as in part A. (**E**) Corresponding data recorded in the presence of 50 nM DDX1 (-RNA) mutant. The histogram is compiled from 142 individual traces. Other details as in part A.

and determined whether it could bind Rev in a fluorescence anisotropy assay. Compared to WT DDX1, this DDX1 mutant binds Rev very weakly (Supplementary Figure S4B). Accordingly, we refer to this construct as DDX1 (-Rev). Notably, the mutations that disrupt Rev binding have no effect on the ability of DDX1 to bind the RRE (27). A representative time trace in the presence of 50 nM of the DDX1 (-Rev) mutant is similar to that in the presence of WT DDX1 (Figure 2C). The distribution of Rev-RRE assembly states apparent in the intensity histogram shows a modest drop in the 2:1 complexes (Figure 2C). The binding kinetics for the first Rev monomer are very similar to those observed in the presence of WT DDX1 (Figure 3D), although there is a small decrease in the amplitude of the fast binding phase (from 94% to 87%, Figure 3D). These results indicate that the L303E and L322E mutations do not significantly alter the ability of DDX1 to promote Rev-RRE assembly.

Since DEAD-box proteins are known to interact with RNA (17,20,28), it is conceivable that DDX1 acts through the RRE to promote Rev-RRE assembly. To test this hypothesis, we created a DDX1 construct that is defective in RNA binding. Based on homology to other DEAD-box proteins, for which co-crystal structures with RNA are known (28), we introduced two point mutations in each of the two putative RNA-binding domains of DDX1 (S295E/R296E/T515E/K516E mutations, Supplementary Figure S4A). Based on a quantitative protein–RNA filter binding assay, we have recently shown that this DDX1 mutant is severely impaired in binding to the RRE (27). Accordingly, we refer to this construct as DDX1 (-RNA). However, this mutant retains the ability to tightly bind Rev (Supplementary Figure S4B). A representative time trace obtained in the presence of 50 nM of the DDX1 (-RNA) mutant (Figure 2E) is very similar to that obtained in the presence of Rev alone (Figure 2B), showing binding of just one or two Rev monomers to the RRE, and the intensity histogram compiled from multiple traces (Figure 2E) is also similar to Rev alone (Figure 2B). Likewise, the first Rev monomer binds slowly to the RRE (Figure 3C), as observed in the presence of Rev alone (Figure 3A). Hence, we con-

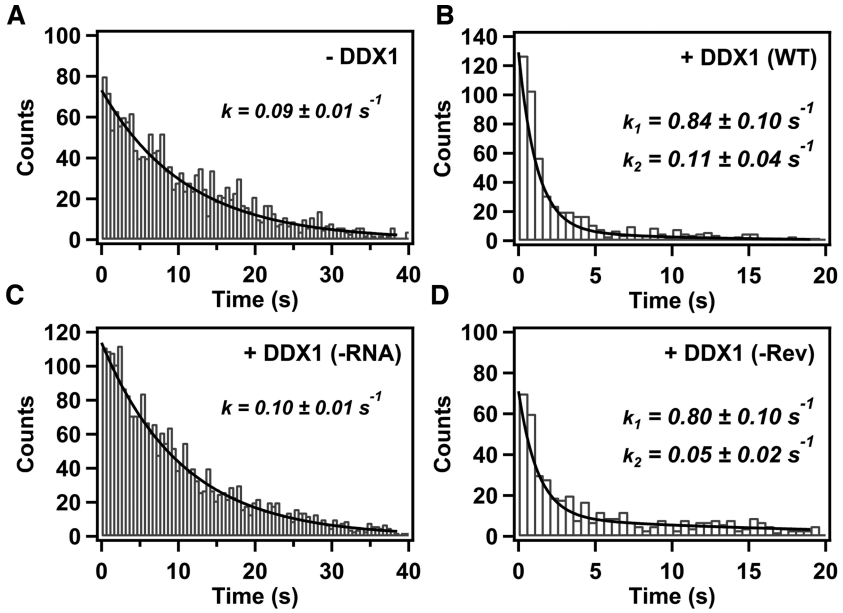

Figure 3. Kinetic analysis of the nucleation step of Rev-RRE assembly. (**A**) Dwell time histogram for binding of the first Rev monomer to the RRE, in the absence of DDX1, compiled from 1072 individual traces. The smooth line is a single exponential fit, with first order rate constant as indicated. (**B**) Corresponding dwell time histogram in the presence of 50 nM WT DDX1, compiled from 481 traces. The smooth line is a bi-exponential fit, with first order rate constants as indicated. The amplitudes of the fast and slow phases are 94 ± 16% and 6 ± 3%, respectively. (**C**) Corresponding dwell time histogram in the presence of 50 nM DDX1 (-RNA) mutant, compiled from 665 traces. The smooth line is the best fit to a single exponential function, with first order rate constant as indicated. (**D**) Corresponding dwell time histogram in the presence of 50 nM DDX1 (-Rev) mutant, compiled from 1110 traces. The smooth line is the best fit to a bi-exponential function, with first order rate constants as indicated. The amplitudes of the fast and slow phases are 87 ± 22% and 13 ± 6%, respectively.

clude that DDX1 must be capable of physically associating with the RRE in order to promote the nucleation step of Rev-RRE assembly.

The second Rev monomer binds to the RRE more rapidly than the first monomer and the association is described by two kinetic phases, with first-order rate constants 1.3 ± 0.2 and 0.16 ± 0.01 s^{-1} (Supplementary Figure S5A). The two kinetic phases may represent different overall conformations of the RRE, as discussed later. Notably, the same two rate constants are observed in the presence of WT DDX1 or any of the DDX1 mutants (Supplementary Figure S5A–D), indicating that DDX1 does not appreciably alter the rate at which the second Rev monomer binds to the RRE. Taken together, the results described here suggest that DDX1 acts primarily through the RRE RNA to influence the nucleation step of Rev-RRE assembly.

Single-molecule Förster resonance energy transfer

In principle, DDX1 could be stably bound to the RRE during Rev binding and oligomerization, or DDX1 might interact transiently with the RRE and not be present during all Rev binding events. To investigate these possibilities, we monitored FRET between Rev and DDX1 on the RRE (Figure 4A). The A555 fluorophore attached to Rev served as the FRET donor and an Alexa 647 (A647) fluorophore attached to DDX1 served as the acceptor. DDX1 was enzymatically labeled within an 11 amino acid peptide tag (termed ybbR) fused to the N-terminus (Supplementary Figure S6). A histogram of A555 emission intensities in the presence of 50 nM A647-labeled DDX1 reveals peaks due to 1:1 and 2:1 Rev-RRE complexes, and a tail extending to higher emission intensity representing unresolved higher order complexes (Supplementary Figure S7). The amplitude of the 2:1 peak relative to the 1:1 peak in Supplementary Figure S7 (62%) is slightly lower than for unlabeled DDX1 in Figure 2C (67%). Consequently, it appears that the A647 fluorophore does not significantly alter the ability of DDX1 to promote oligomerization of Rev on the RRE.

To detect FRET events, we analyzed complexes exhibiting both donor and acceptor emission. A representative pair of donor (green) and acceptor (red) emission time traces obtained with 50 nM A647-labeled WT DDX1 is shown in Figure 4A (middle panel). The abrupt decrease in donor emission at ∼1 s is coincident with the sudden appearance of acceptor emission, indicating that DDX1 binds to the same immobilized RRE molecule and is close enough for FRET to occur from Rev. The acceptor signal disappears at a later time point and the donor signal reverts to it's original value as DDX1 dissociates from the RRE or photobleaches. A histogram of apparent FRET efficiencies compiled from 155 such traces reveals a broad distribution (Supplementary Figure S8A). The breadth of the distribution may arise from the presence of multiple Rev monomers on the RRE, each located at a different distance from DDX1, as well as movements of Rev and/or DDX1 on the RRE. The presence of multiple FRET donors is not accounted for in Equation (2), so the resulting FRET efficiencies should be regarded as apparent values. To confirm that the observed FRET events are due to Rev and DDX1 binding to the RRE, we repeated the smFRET experiments using the DDX1 (-RNA) mutant, which is incapable of binding to the RRE. In this case, the

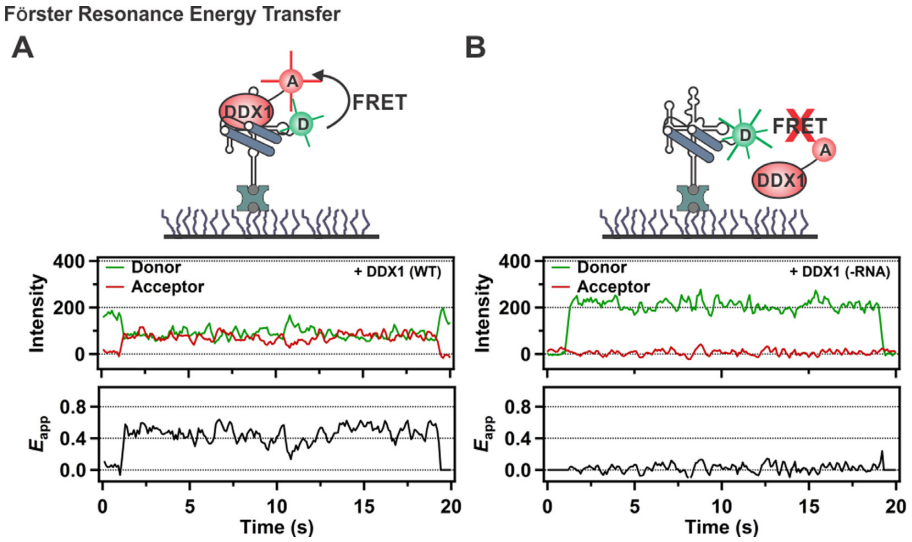

Figure 4. Binding of Rev and DDX1 to the RRE visualized by smFRET. (**A**) The upper panel shows a schematic illustration of FRET between Rev (labeled with A555 donor, shown by the green circle) and WT DDX1 (labeled with A647 acceptor, shown by the red circle). The middle panel shows representative emission intensity versus time traces for the donor (green) and acceptor (red). The lower panel shows the apparent FRET efficiency calculated from Equation (2). (**B**) FRET is not observed with the DDX1 (-RNA) mutant. The middle panel shows binding and dissociation of a single Rev monomer (evident in the donor channel), but no signal in the acceptor channel. Accordingly, the FRET efficiency is close to zero over the entire time course (lower panel).

donor channel reveals discrete jumps in emission intensity as a single Rev monomer binds to or dissociates from the immobilized RRE, but there is no signal in the acceptor channel, indicating the absence of FRET between Rev and the DDX1 mutant, as expected (Figure 4B). Likewise, a histogram compiled from 103 molecules shows only a single peak at zero FRET efficiency (Supplementary Figure S8B). In summary, these results demonstrate that DDX1 and Rev can associate with a single RRE molecule and that the proteins are close enough for FRET to occur.

To obtain information on the kinetics of the DDX1–RRE interaction, we compiled histograms of dwell times spent in the zero-FRET state prior to a DDX1 binding event (appearance of acceptor signal) or dwell times spent in the bound state prior to a dissociation event (disappearance of acceptor signal). The corresponding histograms and single exponential fits are shown in Supplementary Figure S9A and B, respectively. The observed on-rate of $0.21 \pm 0.01\ s^{-1}$ corresponds to a bimolecular rate constant for association of DDX1 with the RRE of $(4.2 \pm 0.2) \times 10^6\ M^{-1}\ s^{-1}$ at the DDX1 concentration used (50 nM labeled DDX1). The apparent off-rate of $0.38 \pm 0.02\ s^{-1}$ is almost 20-fold faster than the rate of photobleaching of the A647 fluorophore ($0.025 \pm 0.001\ s^{-1}$, Supplementary Figure S10), indicating that the loss of the A647 signal is primarily due to dissociation of DDX1 from the RRE. The equilibrium dissociation constant (K_d) for the DDX1–RRE complex calculated from these kinetic parameters ($K_d = 90 \pm 9$ nM) is in accord with the values obtained from equilibrium titrations of the RRE with DDX1 (24–169 nM, depending on buffer conditions (27)).

Analysis of 51 nucleation events (binding of first Rev monomer to the RRE) revealed that FRET occurred from Rev to DDX1 during 18 of these events (35% of total), indicating that DDX1 was present on the RRE. Notably, the observed frequency of the FRET events is fully consistent with the expected occupancy of the RRE by DDX1: based on the K_d value for the DDX1–RRE interaction determined here (90 ± 9 nM) and the 50 nM concentration of labeled DDX1, we expect that 35% of RRE molecules will be occupied by DDX1 under the conditions of our experiments. Since DDX1 is not uniformly labeled with A647, it is possible that unlabeled DDX1 is present during some nucleation events. Based on the known labeling efficiency of DDX1, we calculate that 52% of RRE molecules are occupied by DDX1 (either labeled or unlabeled). Hence, there does not appear to be a strict requirement for DDX1 to be physically present on the RRE during the nucleation process.

DISCUSSION

The single-color assembly experiments reveal that DDX1 acts primarily during the nucleation step of Rev-RRE assembly. The presence of WT DDX1 markedly accelerates binding of the first Rev monomer to the RRE (Figure 3B), but has little effect on the rate at which the second Rev monomer binds (Supplementary Figure S5). Moreover, the vast majority of RRE molecules (94%, Figure 3B) experience this acceleration of Rev binding in the presence of DDX1. By accelerating the nucleation step, DDX1 leads to an increased occurrence of higher assembly states (Figure 2C). Since DDX1 is known to physically interact with both Rev and the RRE (17), the ability of DDX1 to accelerate the nucleation step of Rev-RRE assembly could be mediated either through the Rev protein or the RRE RNA. In our previous study, we attributed the effects of DDX1 to a direct protein–protein interaction between Rev and DDX1, based on the reported high affinity of DDX1 for Rev and the much lower affinity of DDX1 for the RRE (17). However, we could not formally rule out the possibility that DDX1

can also operate through the RRE (12). The tight binding of WT DDX1 to Rev is also observed in the present study ($K_d = 44 \pm 2$ nM, Supplementary Figure S4B). Regardless, the observations reported here for the DDX1 (-Rev) mutant show that DDX1 does not operate through an interaction with Rev. This DDX1 mutant does not bind to Rev under the conditions of our experiments (Supplementary Figure S4B), yet is still capable of accelerating binding of the first Rev monomer to the RRE (Figure 3D) and the distribution of Rev-RRE assembly states is similar to that observed in the presence of WT DDX1 (Figure 2D). Hence, despite the tight binding of WT DDX1 to Rev, this association does not appear to be responsible for DDX1's ability to promote Rev-RRE assembly. Of course, our results do not rule out a role for the DDX1–Rev interaction in other aspects of Rev function, such as targeting Rev to the nucleus (15,18,19).

Two new lines of evidence support a role for a DDX1–RRE interaction during Rev-RRE assembly. First, we find that DDX1 binds to the RRE more tightly ($K_d = 90 \pm 9$ nM) than previously reported ($K_d = 340$ nM, (17)). Quantitative protein–RNA filter binding experiments have also demonstrated a high affinity interaction of DDX1 with the RRE (27). Second, and most compelling, the ability of DDX1 to accelerate Rev-RRE assembly is abrogated by mutations that disrupt RNA binding. The first Rev monomer binds slowly to the RRE in the presence of the DDX1 (-RNA) mutant (Figure 3C), just as observed in the absence of DDX1 (Figure 3A), and the distribution of Rev-RRE assembly states is also similar to that observed in the absence of DDX1 (Figure 2E). These results demonstrate that DDX1 must be capable of physically associating with RNA in order to accelerate the nucleation step of Rev-RRE assembly. The smFRET experiments confirm that DDX1 does indeed bind to the RRE and is located in proximity to Rev (Figure 4A).

There are two models that account for these observations. First, DDX1 could be stably bound to the RRE and facilitate binding of the first Rev monomer, either by stabilizing the RRE in an optimal conformation or through non-specific protein–protein interactions. In this model, which we term the ternary complex model, DDX1 is bound to the RRE before and throughout the nucleation step of Rev-RRE assembly (Figure 5A). In the second model, DDX1 transiently interacts with the RRE and produces an altered RNA conformation that has a higher affinity for Rev and persists after DDX1 has dissociated from the RRE (Figure 5B). In this model, termed the RNA chaperone model, there is no necessity for DDX1 to be physically present on the RRE during Rev-RRE assembly.

One prediction of the ternary complex model is that DDX1 binds to the RRE before Rev (Figure 5A). In fact, we observe that DDX1 does bind to the RRE more rapidly (0.21 s^{-1}, Supplementary Figure S9A) than Rev (0.09 s^{-1}, Figure 3A). However, the model also predicts that DDX1 must be physically present on the RRE to accelerate binding of the first Rev monomer (Figure 5A). Based on the smFRET results, we estimate that DDX1 is present on the RRE during 35–52% of Rev-RRE nucleation events, where the latter estimate accounts for the possible presence of unlabeled DDX1, whereas the single-color assembly data show that 94% of RRE molecules exhibit accelerated Rev binding in the presence of DDX1 (Figure 2B). We conclude that the ternary complex model does not adequately explain the extent to which DDX1 promotes nucleation of Rev-RRE assembly.

However, if DDX1 produces a persistent change in RRE structure, as envisioned in the RNA chaperone model, it is expected that the majority of RRE molecules will exhibit rapid Rev binding, regardless of whether DDX1 is bound to the RRE or not. This is because DDX1 is likely to encounter several RRE molecules before the data recording begins, converting each to a new conformation that results in faster Rev binding. The small fraction of slow binders (6%, Figure 3B) may represent a residual population of RRE molecules that retain their original conformation. It should be noted, however, that since the methods used here do not directly probe the conformation of the RRE, our results neither support nor refute the chaperone model. However, in a recent biochemical study, we have presented evidence that DDX1 induces an RNA structural change within the RRE that persists after dissociation of DDX1 (27). Chemical probing experiments indicate that this structural transition is located within the three-way junction of stem II of the RRE (27), which contains the binding site for the first Rev monomer (11,29). Interestingly, binding of Rev also induced a conformational change within this region (27). If the RNA conformational change is rate limiting for Rev protein binding, then the ability of DDX1 to induce a similar change would necessarily accelerate the nucleation step of Rev-RRE assembly, as we have observed in the present study.

The RNA chaperone activity of DEAD-box proteins is often linked to ATP hydrolysis (reviewed in (30)). However, our results indicate that the ability of DDX1 to accelerate the nucleation step of Rev-RRE assembly does not require the addition of ATP, suggesting that this activity is not linked to ATP hydrolysis. This is consistent with the observation that the RNA chaperone activity of DDX1 is not disrupted by a mutation that eliminates ATPase activity (27). However, we cannot formally rule out the possibility that a trace amount of ATP is carried over during the purification of DDX1 from bacterial cells in our study. It should be noted that ATP-independent RNA unfolding and annealing activities have been described for some DEAD-box helicases (31).

The second Rev monomer binds to the RRE more rapidly (first-order rate constant 1.3 ± 0.2 s^{-1}, Supplementary Figure S5A) than does the nucleating Rev monomer (first-order rate constant 0.09 ± 0.01 s^{-1}, Figure 3A), suggesting that the RRE is pre-organized to bind the second monomer. A recent small angle X-ray scattering study (13) suggests that the RRE adopts an 'A'-shaped architecture that positions the known Rev binding sites in stem IIB and stem IA opposite one other and ~55 Å apart, a distance that matches the separation of the two arginine-rich RNA binding motifs within the crystal structure of a Rev dimer (32). Hence, this RNA structure would enable the second Rev monomer to bind to stem IA while also establishing protein–protein contacts with the nucleating Rev monomer bound to stem IIB. This arrangement would account for the rapid binding of the second Rev monomer during Rev-RRE assembly observed here. Additionally, we also observe a slower kinetic phase during binding of the second Rev monomer

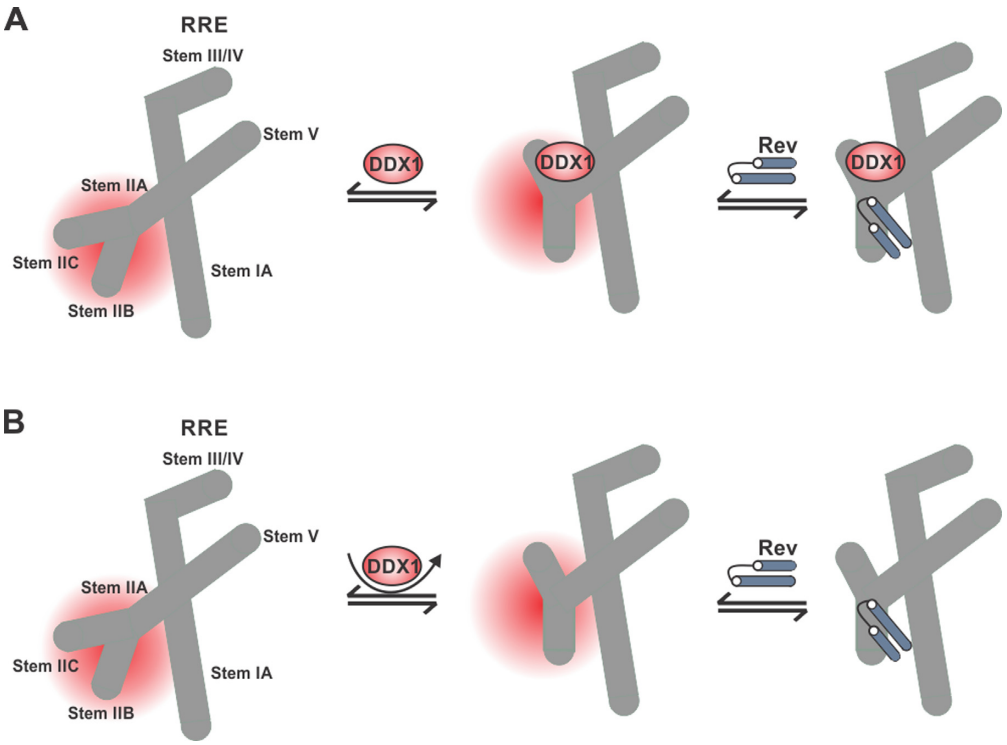

Figure 5. Two models for the role of DDX1 during Rev-RRE assembly. (**A**) Ternary complex model. DDX1 is stably bound to the RRE before and during the nucleation step of Rev-RRE assembly and induces an altered conformation within the stem II three-way junction while bound (shaded in red). The distal region of stem I is not shown. (**B**) RNA chaperone model. DDX1 transiently interacts with the RRE and induces a conformational change within stem II (shaded in red) that persists after DDX1 has dissociated and facilitates the subsequent binding of Rev to the RRE.

(first-order rate constant 0.16 ± 0.01 s^{-1} with 31% amplitude, Supplementary Figure S5A), which may correspond to an alternative RRE conformation in which stems IIB and IA are less optimally positioned for binding of the second Rev monomer. Notably, the kinetic parameters for binding of the second Rev monomer are independent of whether DDX1 is present or not (Supplementary Figure S5), suggesting that DDX1 does not influence the global conformation of the RRE.

In summary, we have shown that DDX1 acts through the RRE RNA to accelerate the nucleation step of Rev-RRE assembly. Our results are most consistent with DDX1 acting as an RNA folding chaperone, producing an altered and persistent RNA structure that has a higher affinity for Rev. To directly test the chaperone model, future smFRET studies employing RRE constructs site-specifically labeled with donor and acceptor probes could be used to detect RNA conformational changes induced by DDX1 and to establish whether these persist after DDX1 has dissociated from the RRE.

SUPPLEMENTARY DATA

Supplementary Data are available at NAR Online.

FUNDING

National Institute of General Medical Sciences and the National Institute of Allergy and Infectious Diseases [P50 GM082545]; California HIV/AIDS Research Program Training Awards-Basic Biomedical Sciences [F12-SRI-210 to R. L.]; American Cancer Society Postdoctoral Fellowship [121633-PF-01-RMC to J.A.H.]. Funding for open access charge: National Institute of General Medical Sciences and the National Institute of Allergy and Infectious Diseases [P50 GM082545].
Conflict of interest statement. None declared.

REFERENCES

1. Pollard,V.W. and Malim,M.H. (1998) The HIV-1 Rev protein. *Annu. Rev. Microbiol.*, **52**, 491–532.
2. Hutten,S. and Kehlenbach,R.H. (2007) CRM1-mediated nuclear export: to the pore and beyond. *Trends Cell Biol.*, **17**, 193–201.
3. Malim,M.H., Bohnlein,S., Hauber,J. and Cullen,B.R. (1989) Functional dissection of the HIV-1 Rev trans-activator–derivation of a trans-dominant repressor of Rev function. *Cell*, **58**, 205–214.
4. Malim,M.H. and Cullen,B.R. (1991) HIV-1 structural gene expression requires the binding of multiple Rev monomers to the viral RRE: implications for HIV-1 latency. *Cell*, **65**, 241–248.
5. Heaphy,S., Dingwall,C., Ernberg,I., Gait,M.J., Green,S.M., Karn,J., Lowe,A.D., Singh,M. and Skinner,M.A. (1990) HIV-1 regulator of virion expression (Rev) protein binds to an RNA stem-loop structure located within the Rev response element region. *Cell*, **60**, 685–693.
6. Huang,X.J., Hope,T.J., Bond,B.L., McDonald,D., Grahl,K. and Parslow,T.G. (1991) Minimal Rev-response element for type 1 human immunodeficiency virus. *J. Virol.*, **65**, 2131–2134.
7. Kjems,J., Brown,M., Chang,D.D. and Sharp,P.A. (1991) Structural analysis of the interaction between the human immunodeficiency virus Rev protein and the Rev response element. *Proc. Natl. Acad. Sci. U.S.A.*, **88**, 683–687.
8. Daly,T.J., Doten,R.C., Rennert,P., Auer,M., Jaksche,H., Donner,A., Fisk,G. and Rusche,J.R. (1993) Biochemical characterization of

binding of multiple HIV-1 Rev monomeric proteins to the Rev responsive element. *Biochemistry*, **32**, 10497–10505.
9. Mann,D.A., Mikaelian,I., Zemmel,R.W., Green,S.M., Lowe,A.D., Kimura,T., Singh,M., Butler,P.J., Gait,M.J. and Karn,J. (1994) A molecular rheostat. Co-operative rev binding to stem I of the rev-response element modulates human immunodeficiency virus type-1 late gene expression. *J. Mol. Biol.*, **241**, 193–207.
10. Daugherty,M.D., D'Orso,I. and Frankel,A.D. (2008) A solution to limited genomic capacity: using adaptable binding surfaces to assemble the functional HIV Rev oligomer on RNA. *Mol. Cell*, **31**, 824–834.
11. Pond,S.J., Ridgeway,W.K., Robertson,R., Wang,J. and Millar,D.P. (2009) HIV-1 Rev protein assembles on viral RNA one molecule at a time. *Proc. Natl. Acad. Sci. U.S.A.*, **106**, 1404–1408.
12. Robertson-Anderson,R.M., Wang,J., Edgcomb,S.P., Carmel,A.B., Williamson,J.R. and Millar,D.P. (2011) Single-molecule studies reveal that DEAD box protein DDX1 promotes oligomerization of HIV-1 Rev on the Rev response element. *J. Mol. Biol.*, **410**, 959–971.
13. Fang,X., Wang,J., O'Carroll,I.P., Mitchell,M., Zuo,X., Wang,Y., Yu,P., Liu,Y., Rausch,J.W., Dyba,M.A. *et al.* (2013) An unusual topological structure of the HIV-1 Rev response element. *Cell*, **155**, 594–605.
14. Cochrane,A.W., McNally,M.T. and Mouland,A.J. (2006) The retrovirus RNA trafficking granule: from birth to maturity. *Retrovirology*, **3**, 18.
15. Fang,J., Kubota,S., Yang,B., Zhou,N., Zhang,H., Godbout,R. and Pomerantz,R.J. (2004) A DEAD box protein facilitates HIV-1 replication as a cellular co-factor of Rev. *Virology*, **330**, 471–480.
16. Naji,S., Ambrus,G., Cimermancic,P., Reyes,J.R., Johnson,J.R., Filbrandt,R., Huber,M.D., Vesely,P., Krogan,N.J., Yates,J.R. 3rd *et al.* (2012) Host cell interactome of HIV-1 Rev includes RNA helicases involved in multiple facets of virus production. *Mol. Cell. Proteomics: MCP*, **11**, doi:10.1074/mcp.M111.015313.
17. Edgcomb,S.P., Carmel,A.B., Naji,S., Ambrus-Aikelin,G., Reyes,J.R., Saphire,A.C., Gerace,L. and Williamson,J.R. (2012) DDX1 is an RNA-dependent ATPase involved in HIV-1 Rev function and virus replication. *J. Mol. Biol.*, **415**, 61–74.
18. Fang,J., Acheampong,E., Dave,R., Wang,F., Mukhtar,M. and Pomerantz,R.J. (2005) The RNA helicase DDX1 is involved in restricted HIV-1 Rev function in human astrocytes. *Virology*, **336**, 299–307.
19. Lin,M.H., Sivakumaran,H., Jones,A., Li,D., Harper,C., Wei,T., Jin,H., Rustanti,L., Meunier,F.A., Spann,K. *et al.* (2014) A HIV-1 Tat mutant protein disrupts HIV-1 Rev function by targeting the DEAD-box RNA helicase DDX1. *Retrovirology*, **11**, 121.
20. Klostermeier,D. (2013) Lifelong companions: RNA helicases and their roles in RNA metabolism. *RNA Biol.*, **10**, 2–3.
21. Steimer,L. and Klostermeier,D. (2012) RNA helicases in infection and disease. *RNA Biol.*, **9**, 751–771.
22. Yin,J., Lin,A.J., Golan,D.E. and Walsh,C.T. (2006) Site-specific protein labeling by Sfp phosphopantetheinyl transferase. *Nat. Protoc.*, **1**, 280–285.
23. Hammond,J.A., Rambo,R.P. and Kieft,J.S. (2010) Multi-domain packing in the aminoacylatable 3′ end of a plant viral RNA. *J. Mol. Biol.*, **399**, 450–463.
24. Lamichhane,R., Solem,A., Black,W. and Rueda,D. (2010) Single-molecule FRET of protein-nucleic acid and protein-protein complexes: surface passivation and immobilization. *Methods (San Diego, Calif.)*, **52**, 192–200.
25. Berezhna,S.Y., Gill,J.P., Lamichhane,R. and Millar,D.P. (2012) Single-molecule Forster resonance energy transfer reveals an innate fidelity checkpoint in DNA polymerase I. *J. Am. Chem. Soc.*, **134**, 11261–11268.
26. McKinney,S.A., Joo,C. and Ha,T. (2006) Analysis of single-molecule FRET trajectories using hidden Markov modeling. *Biophys. J.*, **91**, 1941–1951.
27. Hammond,J.A., Lamichhane,R., Millar,D.P. and Williamson,J.R. (2017) A DEAD-box helicase mediates an RNA structural transition in the HIV-1 rev response element. *J. Mol. Biol.*, **429**, 697–714.
28. Pyle,A.M. (2008) Translocation and unwinding mechanisms of RNA and DNA helicases. *Annu. Rev. Biophys.*, **37**, 317–336.
29. Battiste,J.L., Mao,H., Rao,N.S., Tan,R., Muhandiram,D.R., Kay,L.E., Frankel,A.D. and Williamson,J.R. (1996) Alpha helix-RNA major groove recognition in an HIV-1 rev peptide-RRE RNA complex. *Science (New York, N.Y.)*, **273**, 1547–1551.
30. Jarmoskaite,I. and Russell,R. (2011) DEAD-box proteins as RNA helicases and chaperones. *Wiley Interdiscip. Rev. RNA*, **2**, 135–152.
31. Zhao,X. and Jain,C. (2011) DEAD-box proteins from Escherichia coli exhibit multiple ATP-independent activities. *J. Bacteriol.*, **193**, 2236–2241.
32. DiMattia,M.A., Watts,N.R., Stahl,S.J., Rader,C., Wingfield,P.T., Stuart,D.I., Steven,A.C. and Grimes,J.M. (2010) Implications of the HIV-1 Rev dimer structure at 3.2 A resolution for multimeric binding to the Rev response element. *Proc. Natll. Acad. Sci. U.S.A.*, **107**, 5810–5814.